Inorganic Chemistry

Article

pubs.acs.org/IC

$Pb_2B_3O_{5.5}(OH)_2$ and $[Pb_3(B_3O_7)](NO_3)$: Facile Syntheses of New Lead(II) Borates by Simply Changing the pH Values of the Reaction Systems

Jun-Ling Song, Chun-Li Hu, Xiang Xu, Fang Kong, and Jiang-Gao Mao*

State Key Laboratory of Structural Chemistry, Fujian Institute of Research on the Structure of Matter, Chinese Academy of Sciences, Fuzhou 350002, P. R. China

Supporting Information

ABSTRACT: Using lead metaborate as starting material, by only adjusting pH values of the reaction systems, a series of lead(II) borates were obtained in high yields. The new polar material, namely, $Pb_2B_3O_{5.5}(OH)_2$ (**1**), crystallizes in the noncentrosymmetric space group *Pnn*2 of the orthorhombic system. Its structure features a novel three-dimensional (3D) anionic network with large 14 member rings (MRs) tunnels composed of unique one-dimensional (1D) chains and dimeric B_2O_7 fragments, both of which are built up from solely BO_4 tetrahedra, and the Pb^{2+} cations are located at the above 14-MRs tunnels. The synergistic effect of the stereoactive lone-pairs on Pb^{2+} cations in **1** produces a strong SHG response of ~3× KDP (KH_2PO_4) which is type I phase-matchable. The first example of lead(II) borate nitrate, namely, $[Pb_3(B_3O_7)](NO_3)$ (**2**), crystallizes in space group *Pnma*, and its structures features a 3D lead(II) borate cationic network structure in which $(B_3O_7)^{5-}$ anions are bridged by lead(II) cations, the nitrate anions are isolated, and located at the small voids of the cationic network. Thermal stability and optical properties as well as theoretical calculations based on density functional theory (DFT) methods were also performed.

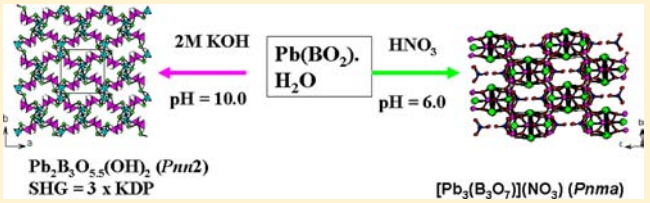

INTRODUCTION

For the past two decades, the development of new second-order nonlinear optical (NLO) materials has attracted tremendous attention because of their important applications in photonic technologies.[1] Currently, a number of NLO materials, including LiB_3O_5 (LBO), β-BaB_2O_4 (BBO), KH_2PO_4 (KDP), and $KTiOPO_4$ (KTP), have been widely used in frequency conversion, optical parameter oscillator (OPO), and signal communication.[2,3] It has been demonstrated that the combination of two types of asymmetric or polar structural building units can result in materials with excellent Second-Harmonic-Generation (SHG) properties. Such polar or asymmetric building groups include π-conjugated system such as borate, nitrate, and carbonate,[4] transition-metal d^0 cation, metal ions with ns^2 lone pair electrons such as Sn^{2+}, Tl^+, Pb^{2+}, and Bi^{3+} ions, and polar displacement of d^{10} cation. Carbonates and nitrates with π-conjugated systems which are similar to triangular BO_3 unit have received considerable attention. Recently, a new series of alkaline−alkaline earth fluoride carbonates with strong SHG response have been reported,[4c,d] and bismuth basic nitrates, for example, $Bi_2O_2[NO_3(OH)]$ with large SHG signal (~6 × KDP) have been reported.[4e] A number of lone pair electrons containing metal borates with excellent SHG properties have been reported, including $Pb_4O(BO_3)_2$,[5a] γ-/δ-BiB_3O_6,[6] $Se_2(B_2O_7)$,[7] $Pb_2B_5O_9I$,[8] $Cd_4BiO(BO_3)_3$,[9] and $Cd_5(BO_3)_3F$.[10] A numbers of lead(II) borates with clusters,[11] chains,[12] layers,[5b] or three-dimensional (3D) famework structures[5a,13,14] have been reported. Lead(II) borates with highly asymmetric bonds favor SHG activity based on bond polarizability theory.[15] For example, PbB_4O_7 with a 3D network structure has been widely studied because of its highly asymmetric bonding, and high mechanical and fairly low hygroscopic characteristics.[13] In the most cases, these lead(II) borates were usually prepared by high temperature solid state reactions or by a complicated hydrothermal synthesis method. For example, $Pb_6B_{11}O_{18}(OH)_9$[12] and $Pb_5(B_3O_8OH)_3{\cdot}H_2O$[5b] with noncentrosymmetric structures were previously synthesized in the hydrothermal system at high temperature (270 °C) and high pressure (100 bar) or in a complicated hydrothermal system (including organic ethylenediamine in the crystallization system and acetic to obtain the target crystals), respectively. Molten boric acid as a reactive flux media has been used as a facile method for producing lanthanide nitratoborates[16a−c] and lanthanide/actinide borates.[16d−f] Compared with these methods, hydrothermal syntheses under moderate temperatures have great advantages for the preparations of metastable crystalline materials.[17] Moreover, different reaction conditions such as temperature, counterion, stoichiometry, and pH value of the reaction media can result in the metal borates with various types of structures.[17,18] A number of polyborates exist in aqueous borate solutions depending on experimental conditions.[19] Besides, additional anions such as halides and perchlorate have been also introduced to the metal borate systems to create much more structural diversity.[16]

Received: May 10, 2013
Published: July 8, 2013

   dx.doi.org/10.1021/ic401175r | *Inorg. Chem.* 2013, 52, 8979−8986

To explore new metal borates with high SHG efficiencies, we deem that the studies on the reaction conditions of the borate systems are also very interesting and important for understanding the structure−property relationships. In this work, we hope to explore new lead(II) borates by using a facile hydrothermal synthesis methods under different pH values, and we also try to introduce nitrate groups with a triangular π-conjugated system to the lead(II) borates. Based on these ideas, a new polar material, namely, $Pb_2B_3O_{5.5}(OH)_2$ (**1**), with a strong SHG response of ∼3× KDP (KH_2PO_4), and the first lead(II) borate nitrate, namely, $[Pb_3(B_3O_7)](NO_3)$ (**2**), have been also isolated. Herein we report their syntheses, electronic crystal structures, and optical properties.

EXPERIMENTAL SECTION

Materials and Instruments. $Pb(BO_2)_2{\cdot}H_2O$ (AR, 99.0%), KOH (AR, 99.0%), and dilute HNO_3 solution (∼30%) were purchased from the Shanghai Reagent Factory without further purification. IR spectra were recorded on a Magna 750 FT-IR spectrometer as KBr pellets in the range of 4000−450 cm^{-1}. Microprobe elemental analyses for the Pb, B, and N elements were performed on a field-emission scanning electron microscope (FESEM, JSM6700F) equipped with an energy-dispersive X-ray spectroscope (EDS, Oxford INCA). Powder X-ray diffraction (XRD) patterns were collected on a Rigaku MiniFlex II diffractometer using Cu−Kα radiation in the angular range of 2θ = 5−85° with a step size of 0.05°. The inductively coupled plasma (ICP) elemental analyses of $Pb_2B_3O_{5.5}(OH)_2$ and $[Pb_3(B_3O_7)](NO_3)$ were measured using an Ultima 2 simultaneous inductively coupled plasma-optical emission spectrometer. Optical diffuse-reflectance spectra were measured at room temperature with a PE Lambda 900 UV−vis−NIR spectrophotometer. The $BaSO_4$ plate was used as a standard (100% reflectance). The absorption spectrum was calculated from reflectance spectrum using the Kubelka−Munk function: $\alpha/S = (1 - R)^2/2R$, where α is the absorption coefficient, S is the scattering coefficient, which is practically wavelength-independent when the particle size is larger than 5 μm, and R is the reflectance.[20] Thermogravimetric analysis (TGA) was carried out with a NETZSCH STA 449C unit at a heating rate of 15 °C/min under nitrogen atmosphere. Measurements of the powder frequency-doubling effect for $Pb_2B_3O_{5.5}(OH)_2$ were carried out by means of the modified method of Kurtz and Perry.[21] 1064 nm radiation generated by a Q-switched Nd:YAG solid-state laser was used as the fundamental frequency light. The SHG wavelength is 532 nm. The SHG efficiency has been shown to depend strongly on the particle size; thus, the sample was ground and sieved into several distinct particle size ranges (25−45, 45−53, 53−75, 75−105, 105−150, and 150−210 μm). Sieved KDP powder (150−210 μm) was used as a reference material to assume the SHG effect.

*Preparation of $Pb_2B_3O_{5.5}(OH)_2$ (**1**).* A mixture of $Pb(BO_2)_2{\cdot}H_2O$ (0.716 g, 2.3 mmol) and H_2O (6.0 mL) with pH value adjusted to 10.0 by the addition of a few drops of 2 M KOH was sealed in an autoclave equipped with a Teflon liner (20 mL) and heated at 210 °C for 4 days. The final pH value is 9.5. Needle-like crystals of $Pb_2B_3O_{5.5}(OH)_2$ were collected in a yield of about 90% based on Pb. ICP elemental analyses gave a B content of 5.51%, which is close to the calculated value of 5.70% based on single crystal X-ray diffraction analyses. IR data (KBr cm^{-1}): 3440 (br, m), 1435 (m), 1359 (m), 1299 (s), 1219 (vs), 1188 (s), 1143 (m), 1108 (s), 891 (m), 831 (w), 704 (m), 628 (m), 543 (m), 417 (w).

*Preparation of $[Pb_3(B_3O_7)](NO_3)$ (**2**).* A mixture of $Pb(BO_2)_2{\cdot}H_2O$ (0.716 g, 2.3 mmol) and H_2O (6.0 mL) with pH value adjusted to 6.0 by addition of a few drops of HNO_3 solution (∼30%) was sealed in an autoclave equipped with a Teflon liner (20 mL) and heated at 210 °C for 4 days. The final pH value of the reaction system is 5.5. Large pale-yellow prism-like crystals of $[Pb_3(B_3O_7)](NO_3)$ were obtained in a yield of about 80% based on Pb. The EDS analysis of $[Pb_3(B_3O_7)](NO_3)$ confirms the Pb/N elemental composition. ICP analysis gave B content of 3.61%, which is close to that calculated value of 3.92% base on single crystal X-ray structural analyses. IR data (KBr cm^{-1}): 1340 (vs), 1216 (m), 997 (m), 924 (s), 868 (s), 733 (w), 672 (m), 631 (w), 598 (w), 582 (w), 553 (w), 492 (m), 446 (m), 413 (w).

X-ray Crystallography. Single Crystal X-ray diffraction data collections for both compounds were performed on a Supernova CCD diffractometer equipped with graphite-monochromated Mo−Kα radiation (λ = 0.71073 Å) at 293 K. The data sets were corrected for Lorentz and polarization factors as well as absorption by the multiscan method.[22a] Both structures were solved by the direct methods and refined by full matrix least-squares fitting on F^2 using SHELX-97.[22b] All non-hydrogen atoms were refined with anisotropic thermal parameters except for B(1) in $[Pb_3(B_3O_7)](NO_3)$ and B(3) in $Pb_2B_3O_{5.5}(OH)_2$, which were refined with 'ISOR' constraints. Without these constraints, their displacement parameters will be abnormally small. O(1) and O(6) in $Pb_2B_3O_{5.5}(OH)_2$ are assigned to be hydroxyl groups based on the requirements of charge balance and bond valence calculations; their calculated bond valences are −1.09.[23] All hydrogen atoms are located at geometrically calculated positions and refined with isotropic thermal parameters. The Flack parameter of $Pb_2B_3O_{5.5}(OH)_2$ was refined to be 0.0005, indicative of the correctness of its absolute structure. Both structures were also checked for possible missing symmetry with PLATON.[22c] Crystallographic data and structural refinements for the two compounds are summarized in Table 1. Important bond distances are listed in Table 2. More details on the crystallographic studies as well as atomic displacement parameters are given as Supporting Information.

Table 1. Crystal Data and Structural Refinements for $Pb_2B_3O_{5.5}(OH)_2$ and $[Pb_3(B_3O_7)](NO_3)$[a]

formula	$Pb_2B_3O_{5.5}(OH)_2$	$[Pb_3(B_3O_7)](NO_3)$
fw	568.83	828.01
space group	*Pnn*2	*Pnma*
a/Å	11.5824(7)	10.3481(5)
b/Å	11.7664(7)	7.8908(4)
c/Å	4.5657(2)	11.2123(5)
V/Å^3	622.23(6)	915.54(8)
Z	4	4
D_{calcd}/g cm^{-3}	6.072	6.007
μ(Mo−Kα)/mm^{-1}	54.041	55.078
GOF on F^2	0.993	1.132
Flack factor	0.0005	N/A
R_1, wR_2 ($I > 2\sigma(I)$)[a]	0.0217, 0.0385	0.0275, 0.0663
R_1, wR_2 (all data)	0.0242, 0.0395	0.0295, 0.0678

[a] $R^1 = \sum||F_o| - |F_c||/\sum|F_o|$, $wR_2 = \{\sum[w(F_o^2 - F_c^2)^2]/\sum[w(F_o^2)^2]\}^{1/2}$.

Computational Descriptions. Single-crystal structural data of $Pb_2B_3O_{5.5}(OH)_2$ (**1**) and $[Pb_3(B_3O_7)](NO_3)$ (**2**) were used for the theoretical calculations. The electronic structures including band structure and density of states (DOS) calculations were performed using a plane-wave basis set and pseudopotentials within density functional theory (DFT) implemented in the total-energy code CASTEP.[24] The exchange and correlation effects were treated by Perdew−Burke−Ernzerhof (PBE) in the generalized gradient approximation (GGA).[25] The interactions between the ionic cores and the valence electrons were described by the norm-conserving pseudopotential.[26] The following valence-electron configurations were considered in the computation: Pb-4$s^2$4$p^6$5s^1, B-2$s^2$2p^1, O-2$s^2$2p^4, N-2$s^2$2p^3, and H-1s^1. The number of plane waves included in the basis sets was determined by the cutoff energy of 700 and 820 eV, respectively, for $Pb_2B_3O_{5.5}(OH)_2$ and $[Pb_3(B_3O_7)](NO_3)$. In addition, the numerical integration of the Brillouin zone was performed using Monkhorst−Pack k-point sampling of 2 × 2 × 5 and 2 × 3 × 2, respectively. The other parameters and convergence criteria were the default values of the CASTEP code.

dx.doi.org/10.1021/ic401175r | Inorg. Chem. 2013, 52, 8979−8986

Table 2. Selected Bond Distances (Å) for $Pb_2B_3O_{5.5}(OH)_2$ and $[Pb_3(B_3O_7)](NO_3)$[a]

	$Pb_2B_3O_{5.5}(OH)_2$		
Pb(1)−O(7)	2.253(6)	B(1)−O(2)	1.485(14)
Pb(1)−O(5)#1	2.278(7)	B(1)−O(4)	1.502(16)
Pb(1)−O(4)	2.330(7)	B(2)−O(6)	1.464(12)
Pb(1)−O(3)	2.957(7)	B(2)−O(4)	1.480(19)
Pb(2)−O(7)	2.286(6)	B(2)−O(3)#5	1.481(17)
Pb(2)−O(2)#2	2.374(7)	B(2)−O(5)	1.511(12)
Pb(2)−O(8)#1	2.503(6)	B(3)−O(7)	1.40(2)
Pb(2)−O(3)#3	2.568(7)	B(3)−O(5)	1.482(13)
Pb(2)−O(7)#4	2.675(6)	B(3)−O(2)#3	1.481(13)
B(1)−O(3)	1.46(2)	B(3)−O(8)	1.517(12)
B(1)−O(1)	1.461(12)		
	$[Pb_3(B_3O_7)](NO_3)$		
Pb(1)−O(2)#1	2.271(6)	Pb(2)−O(3)#1	2.263(9)
Pb(1)−O(4)#2	2.321(6)	Pb(2)−O(4)	2.279(7)
Pb(1)−O(3)#3	2.354(5)	Pb(2)−O(4)#4	2.279(7)
Pb(1)−O(1)#1	3.005(7)	Pb(2)−O(2)#1	2.799(1)
Pb(1)−O(1)#3	3.030(7)	B(2)−O(4)	1.360(1)
B(1)−O(2)	1.460(2)	B(2)−O(5)	1.392(1)
B(1)−O(1)	1.471(1)	N(1)−O(6)	1.22(2)
B(1)−O(1)#6	1.471(1)	N(1)−O(7)#6	1.250(1)
B(1)−O(3)	1.479(2)	N(1)−O(7)	1.250(1)
B(2)−O(1)	1.375(1)		

[a]Symmetry transformations used to generate equivalent atoms. For $Pb_2B_3O_{5.5}(OH)_2$: #1 *x*, *y*, *z*+1; #2 *x*+1/2, −*y*+3/2, *z*+1/2; #3 *x*+1/2, −*y*+3/2, *z*−1/2; #4 −*x*+1, −*y*+1, *z*. For $[Pb_3(B_3O_7)](NO_3)$: #1 −*x*+1/2, −*y*+1, *z*+1/2 ; #2 *x*+1/2, *y*, −*z*+3/2; #3 −*x*+1, −*y*+1, −*z*+1; #4 *x*, −*y*+3/2, *z*; #5 −*x*+1, −*y*, −*z*+1; #6 *x*, −*y*+1/2, *z*.

RESULTS AND DISCUSSION

The previous synthetic methods for other lead(II) borates require high temperature or high pressure. For example, $Pb_5(B_3O_8OH)_3{\cdot}H_2O$ was previously synthesized by the hydrothermal reactions at high temperature (270 °C) and high pressure (100 bar);[5b] and $Pb_6B_{11}O_{18}(OH)_9$ was prepared by using a complicated hydrothermal system (including organic ethylenediamine in the crystallization system and acetic to produce the target crystals).[12] In our work, we adopt a much simpler and cleaner method which uses lead(II) metaborate as the starting material and only adjust pH values of the reaction system. This synthetic method resulted in the isolation of four different lead(II) borates, among which $Pb_2B_3O_{5.5}(OH)_2$ and $[Pb_3(B_3O_7)](NO_3)$ are new. It is worth noting that the initial pH value of the reaction system is critical for the growth of these crystalline materials. Different crystals obtained under different initial pH values are shown in Chart 1. The pH value was adjusted by adding a few drops dilute HNO_3 solution (∼30%) and 2 M KOH solution, respectively. We first carried out the reaction at a pH value of 1.0, and colorless hexagon tile-shaped crystals of $Pb_5(B_3O_8OH)_3{\cdot}H_2O$[5b] were obtained in a yield of about 30% based on Pb, combined with a small amount of white powder of $Pb_6B_{11}O_{18}(OH)_9$.[12] When the pH value of the same reaction system was adjusted to 7.0, colorless prism-shaped crystals of $Pb_6B_{11}O_{18}(OH)_9$[12] were obtained in a yield of about 85% based on Pb. When the pH value was adjusted to 6.0, colorless brick-shaped crystals of $[Pb_3(B_3O_7)](NO_3)$ (**2**) were obtained in a yield of about 80% based on Pb. If the pH value of the reaction system was raised to 10.0, crystals of $Pb_2B_3O_{5.5}(OH)_2$ (**1**) were isolated. Only red PbO crystals were formed when the reaction was carried out under more basic media (pH = 12.0). All of the products were washed with hot water and ethanol, and then dried in air. Their purities were confirmed by power XRD diffraction studies (Supporting Information, Figure S1).

Chart 1. Products Obtained at Different pH Values of 1.0, 6.0, 7.0, 10.0, and 12.0

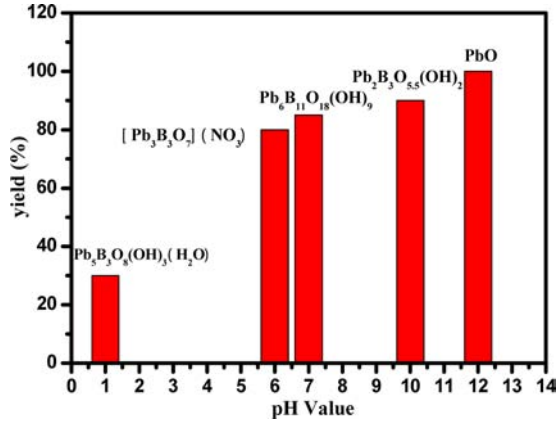

Crystal Structure of $Pb_2B_3O_{5.5}(OH)_2$ (1). $Pb_2B_3O_{5.5}(OH)_2$ (**1**) crystallizes in the noncentrosymmetric and polar space group *Pnn*2. Its structure features a 3D anionic borate framework with large one-dimensional (1D) tunnels of 14-member rings (MRs) along the *c*-axis, and the lead(II) cations are capped on the walls of the above 1D tunnels (see Figure 1a). The asymmetric unit of $Pb_2B_3O_{5.5}(OH)_2$ contains two unique Pb and three unique B atoms. Pb(1) is four coordinated whereas Pb(2) atoms is five coordinated. These PbO_4 and PbO_5 polyhedra are highly distorted because of the lone pair electrons of the lead(II) cations, the Pb−O bond lengths range from 2.253(6) to 2.957(7) Å and O−Pb−O vary from 73.8 (2) to 129.86(19)°, which are comparable to those reported in other lead(II) borates.[11−14] Both B(1) and B (2) are tetrahedrally coordinated by one hydroxyl group and three oxo anions whereas B(3) is tetrahedrally coordinated by four oxo anions. These tetrahedra are slightly distorted with the B−O distances ranging from 1.40(2) to 1.517(12) Å and B−O−B bond angles in the range of 100.7 to 115.8(10)°, which are in good agreement with those reported previously in other lead borates.[11−14,16] The calculated total bond valences for Pb1, Pb2, B1, B2, and B3 are 1.98, 1.98, 3.01, 2.95, and 3.07, respectively. O(1) and O(6) atoms are assigned to be hydroxyl group with the calculated bond valences of −1.09.[23]

The above $B(1)O_3(OH)$ and $B(2)O_3(OH)$ tetrahedra are corner-sharing into 1D $[B_2O_4(OH)_2]$ chains by corner-sharing along the *c*-axis whereas each pair of $B(3)O_4$ tetrahedra form a $[B_2O_7]^{8-}$ dimer by vertex-sharing (Figure 1b). Each B_2O_7 dimer connects with four $[B_2O_4(OH)_2]$ chains by corner-sharing, resulting in the formation of a novel 3D network with 1D tunnels of fourteen-membered rings along [001] (Figure 1b). The size of the tunnel is estimated to be 13.97 × 5.74 Å^2. If the 1D chain of $B(1)O_3(OH)$ and $B(2)O_3(OH)$ tetrahedra is considered to be based on "$B(1,2)_2O_5(OH)_2$" dimeric units, each $B_2O_5(OH)_2$ connects with two neighboring $B(1,2)_2O_5(OH)_2$ units and two $B(3)_2O_7$ units, hence both $B(1,2)_2O_5(OH)_2$ and $B(3)_2O_7$ dimeric units are 4-connected nodes, TOPOS analysis reveals that the above 3D borate framework is a new 4,4-connected network with the Schläfli symbol of $\{6^4;8;10\}^2\{6^6\}$ (Figure 1c).[27] The lead(II) cations are located at the above 1D tunnels (Figure 1a). It is interesting

dx.doi.org/10.1021/ic401175r | Inorg. Chem. 2013, 52, 8979−8986

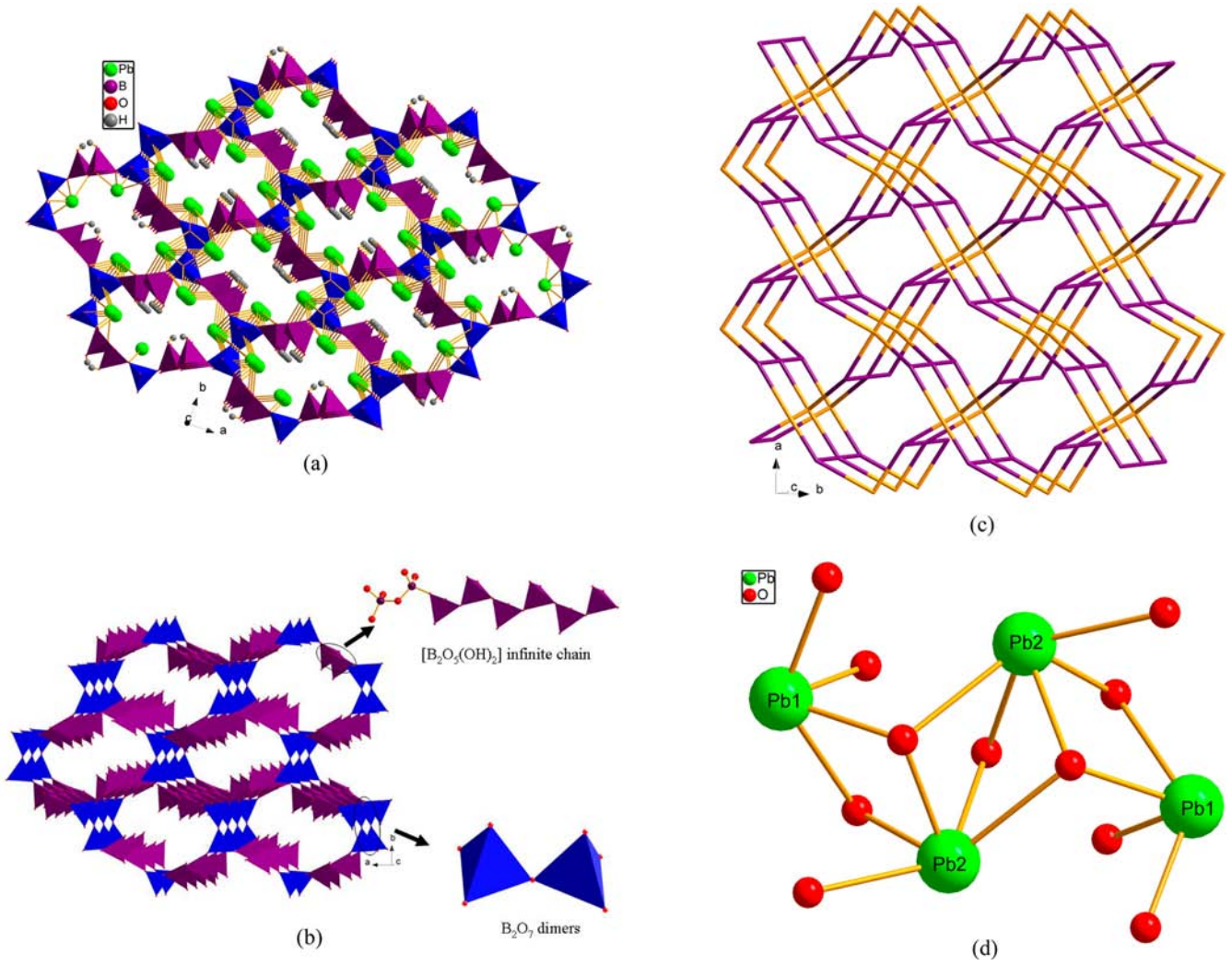

Figure 1. View of the crystal structure of $Pb_2B_3O_{5.5}(OH)_2$ (**1**) along the *c* axis (a), a 3D borate anionic network composed of 1D chains of corner sharing $B(1)O_4$ and $B(2)O_4$ tetrahedra that are further interconnected $B(3)_2O_7$ dimers; $BO_3(OH)$ and $B(3)O_4$ tetrahedra are shaded in purple and blue, respectively; H atoms are omited for clarity (b), topological view of a new 4,4-connected network with the Schläfli symbol of $\{6^4;8;10\}^2\{6^6\}$; the organge and purple balls represent the B_2O_7 dimers and $B_2O_5(OH)_2$, respectively (c), and a Pb_4O_{11} tetranuclear cluster in $Pb_2B_3O_{5.5}(OH)_2$ (d).

to note that $Pb(1)O_4$ and $Pb(2)O_5$ polyhedra are interconnected via edge- and face-sharing into a novel Pb_4O_{11} tetranuclear cluster (Figure 1d).

Crystal Structure of $[Pb_3(B_3O_7)](NO_3)$ (2). $[Pb_3(B_3O_7)](NO_3)$ (**2**) represents the first mixed anion lead(II) borate-nitrate. It crystallizes in the orthorhombic centrosymmetric space group *Pnma*. The structure of $[Pb_3(B_3O_7)](NO_3)$ (**2**) features a 3D structure composed of B_3O_7 polyanions that are interconnected by lead(II) cations, forming 1D tunnels of 6-member rings (MRs) that are filled by isolated nitrate anions (Figure 2a). There are two unique lead(II) and two unique boron atoms in the asymmetric unit of $[Pb_3(B_3O_7)](NO_3)$. Pb(1) is five coordinated by five oxygen atoms, the Pb−O bond distances vary from 2.271(6) to 3.030(7) Å, and the O−Pb−O bond angles range from 50.5(2)−156.0(2)°. The Pb(2) ion is four coordinated by four oxygen atoms with Pb−O distances ranging from 2.268(9)−2.799(1) Å and O−Pb−O bond angles falling in the range of 54.9(3)−112.2(2)°. Both $Pb(1)O_5$ and $Pb(2)O_4$ polyhedra are highly distorted because of the lone pair electrons of the lead(II) ion. Two $Pb(1)O_5$ and one $Pb(2)O_4$ polyhedra are interconnected by edge-sharing into an incomplete cubane-like Pb_3O_4 cluster, and neighboring Pb_3O_4

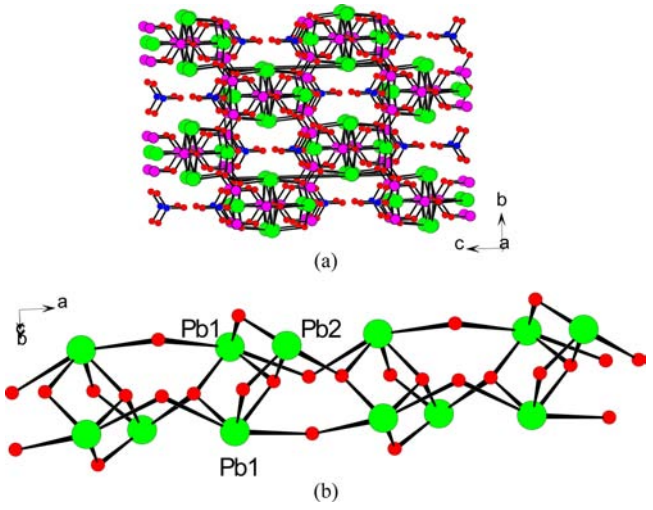

Figure 2. View of the structure of $[Pb_3(B_3O_7)](NO_3)$ along the *a* axis (a), and an infinite lead(II) oxide chain composed of Pb_3O_4 clusters along the *a*-axis (b). Pb, B, N, and O atoms are drawn as green, purple, blue, and red circles, respectively.

dx.doi.org/10.1021/ic401175r | *Inorg. Chem.* 2013, 52, 8979−8986

clusters are further interconnected by a number of intercluster Pb−O−Pb bridges into an infinite $[Pb_3O_6]$ chain along the *a* axis (Figure 2b). B(1) atom is in a BO_4 tetrahedral geometry whereas B(2) is in a BO_3 triangular coordination geometry. Two BO_3 groups and one BO_4 tetrahedron form a common $[B_3O_7]^{5-}$ polyanion. The B−O bonds and B−O−B bond angles for the $B(2)O_3$ unit are in the range of 1.360(1)−1.392(1) Å and 118.6(9)−121.1(9)°, respectively. In contrast, the B−O bonds and B−O−B bond angles for the $B(1)O_4$ unit range from 1.460(2)−1.479(2) Å and 107.5(7)−112.9(1)°, respectively. These bond distances and angles are close to those reported in other borates.[11−14,16] The nitrate anions are located at the above channels of the structure and remain non-coordinated, which is similar to those reported in lanthanide nitratoborates.[16] The calculated total bond valences for Pb1, Pb2, B1, B2, and N1 are 1.91, 2.00, 3.07, 2.97 and 5.05, respectively, indicating that they are in oxidation states of +2, +3, and +5, respectively.[23]

Optical Properties. $Pb_2B_3O_{5.5}(OH)_2$ and $[Pb_3(B_3O_7)](NO_3)$ show strong absorption in the region of 200 to 367 nm and 200 to 408 nm, respectively (Supporting Information, Figure S2). Both compounds show little absorption in the range of 410−2500 nm. The optical diffuse reflectance spectrum measurements indicate that $Pb_2B_3O_{5.5}(OH)_2$ and $[Pb_3(B_3O_7)](NO_3)$ are wide band gap semiconductors with optical band gaps of 4.42 and 3.64 eV, respectively (Supporting Information, Figure S3). Hence, $Pb_2B_3O_{5.5}(OH)_2$ and $[Pb_3(B_3O_7)](NO_3)$ are transparent in the range of 0.40−2.50 μm. IR spectra of these two compounds display some features similar to those of other metal borates (Supporting Information, Figure S4).[12−14,16] As shown in Supporting Information, Figure S4, the broad absorption band at 3440 cm^{-1} confirms the presence of OH groups in $Pb_2B_3O_{5.5}(OH)_2$, and the bands between 1400 and 1100 cm^{-1} are due to the in-plane bending of the B−O−H mode. The bands between 700−1100 cm^{-1} show the obviously characteristic peaks of the asymmetric stretching of tetrahedral BO_4 groups and the symmetric stretch of BO_4 groups. The absorptions below 630 cm^{-1} can be assigned to the bands of tetrahedral B deformation modes. These assignments are consistent with those reported in other metal borates.[28,29] For $[Pb_3(B_3O_7)](NO_3)$, the strong absorption peaks were observed at 1340 cm^{-1} and 868 cm^{-1}, which can be attributed to the overlap of the asymmetric stretching of BO_3 with the stretching vibration or bending vibrations of NO_3, respectively, whereas the absorption peaks at 1216 cm^{-1} and the bands between 1000 and 870 cm^{-1} can be attributed to the asymmetric and symmetric stretch of BO_3 groups (Supporting Information, Figure S4). Similar to the triangular borate group BO_3 in $Pb_5(B_3O_8OH)_3{\cdot}H_2O$,[5b] the peaks at 733 and 672 cm^{-1} are out-of-plane bending of B−O in BO_3. The bending vibrations of BO_3 and BO_4 are also shown in the 400−630 cm^{-1} range; because of some overlaps in these regions, it is very hard to assign these bands in detail. IR spectrum confirmed the coexistence of NO_3, BO_3, and BO_4 groups in $Pb_3B_3O_7(NO_3)$, which is in consistent with the results obtained from crystallographic studies.

TGA Studies. Thermogravimetric analysis (TGA) of $Pb_2B_3O_{5.5}(OH)_2$ shows a weight loss of about 2.07% in the range from 260 to 755 °C under nitrogen atmosphere, which corresponds to the removal of water molecules formed by condensation of hydroxyl groups (calculated value 3.16%), and two distinct endothermic peaks at around 547 and 582 °C can be found in the DTA curves. After dehydration, it loses weight continuously up to about 1000 °C (Supporting Information, Figure S5a) and then the material becomes amorphous. The total weight loss of about is 6.33%. TGA studies indicate that $[Pb_3(B_3O_7)](NO_3)$ is thermally stable up to about 478 °C under nitrogen atomsphere (Supporting Information, Figure S5b). Then it displays one step of weight loss in the temperature range of 478−578 °C, corresponding to the decomposition of NO_3^- group, which is in agreement with the one apparent endothermic peak observed at 570 °C in the thermal analysis (DTA) diagram. The observed total weight loss is 6.52%. The final residuals are not characterized because of their amorphous nature.

SHG Properties. SHG measurements on a 1064 nm Q-switch laser with the sieved powder samples revealed that $Pb_2B_3O_{5.5}(OH)_2$ exhibits a strong SHG response of 3.0 times that of KDP, which is about ~2.1 times that of $Pb_6B_{11}O_{18}(OH)_9$.[12] The particle size vs SHG efficiency plot indicates that $Pb_2B_3O_{5.5}(OH)_2$ is type I phase-matchable (Figure 3). According to anionic group theory,[4] the

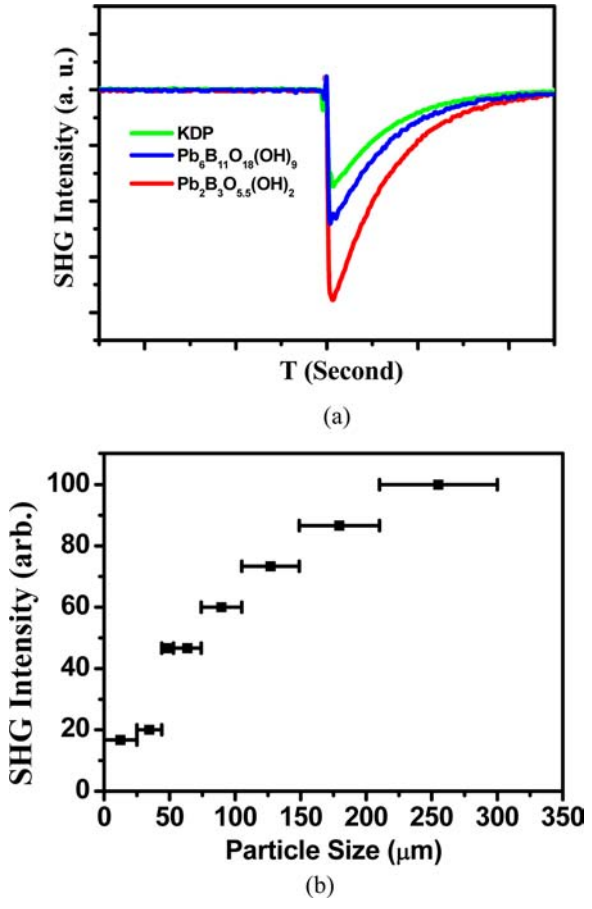

Figure 3. Oscilloscope traces of the SHG signals for the powders (270−325 μm) of KDP, $Pb_6B_{11}O_{18}(OH)_9$, and $Pb_2B_3O_{5.5}(OH)_2$ (a), and the phase-matching curve for $Pb_2B_3O_{5.5}(OH)_2$ (b). The curve drawn is to guide the eye and not a fit to the data.

contribution of BO_4 tetrahedra to the SHG response is small, thus the SHG effect of $Pb_2B_3O_{5.5}(OH)_2$ should be mainly originating from Pb−O bonding.[13] To better understand the magnitude and direction of the dipole moments, the local dipole moments for the PbO_4 and PbO_5 polyhedra and the net dipole moment within a unit cell for $Pb_2B_3O_{5.5}(OH)_2$ were calculated by using a method reported earlier.[30,31] Calculation

dx.doi.org/10.1021/ic401175r | Inorg. Chem. 2013, 52, 8979−8986

results showed that the *x*, *y*, and *z*-component of the polarizations within a unit cell for four $Pb(1)O_4$ polyhedra are 2× (±1.51 D), 2× (±9.10 D), and 4 × (−1.39) D, respectively, and those for the four $Pb(2)O_5$ polyhedra are 2× (±7.83 D), 2× (±3.68 D), and 4× (−0.94) D, respectively. Thus the *x*- and *y*-components of the polarizations canceled out completely, whereas those of the *z*-components constructively add to produce a moderate net dipole moment of 9.32 D along the *c* axis (Supporting Information, Figure S6). Thus, the synergistic effect of the stereoactive lone-pairs on Pb^{2+} cations in $Pb_2B_3O_{5.5}(OH)_2$ produces a moderate strong SHG response.

Theoretical Studies. To gain further insight the bonding interactions in both $Pb_2B_3O_{5.5}(OH)_2$ and $[Pb_3(B_3O_7)](NO_3)$, theoretical calculations were made based on DFT methods. The calculated band structures of $Pb_2B_3O_{5.5}(OH)_2$ and $[Pb_3(B_3O_7)](NO_3)$ along high-symmetry points of the first Brillouin zone are plotted in Figure 4. It is clear that both the

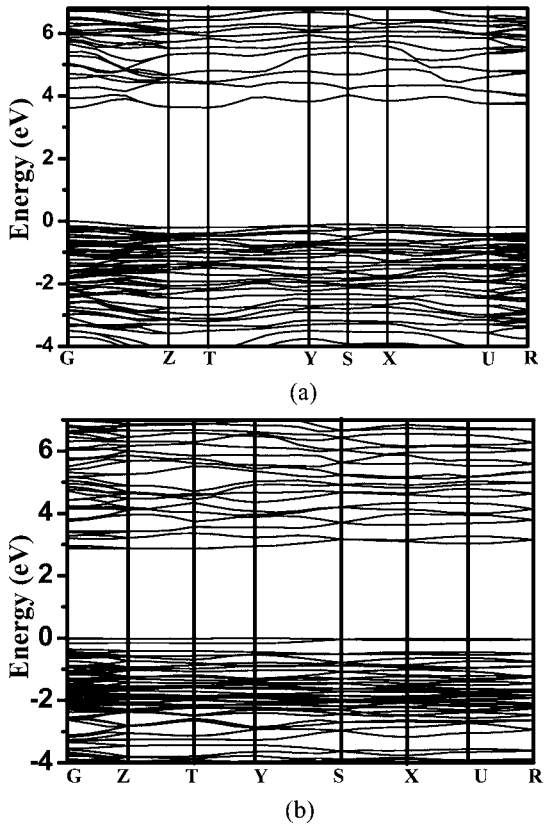

Figure 4. Calculated band structure of $Pb_2B_3O_{5.5}(OH)_2$ (a) and $[Pb_3(B_3O_7)](NO_3)$ (b).

lowest conduction band and the highest valence band are localized at the G point, hence both $Pb_2B_3O_{5.5}(OH)_2$ and $[Pb_3(B_3O_7)](NO_3)$ are direct band gap semiconductors. The calculated band gaps of 3.60 and 2.93 eV for $Pb_2B_3O_{5.5}(OH)_2$ and $[Pb_3(B_3O_7)](NO_3)$ are much smaller than their experimental values. This is not surprising, because DFT-GGA does not accurately describe the eigenvalues of the electronic states, resulting in quantitative underestimation of band gaps.[31] The bands can be assigned according to the total and partial DOS, as plotted in Figure 5. For $Pb_2B_3O_{5.5}(OH)_2$, the valence band in the range from −21.0 to −16.0 eV arises from mostly O-2s, mixing with a small amount of B-2s2p and H-1s states. The peak localized around −15.0 eV is mostly contributed by

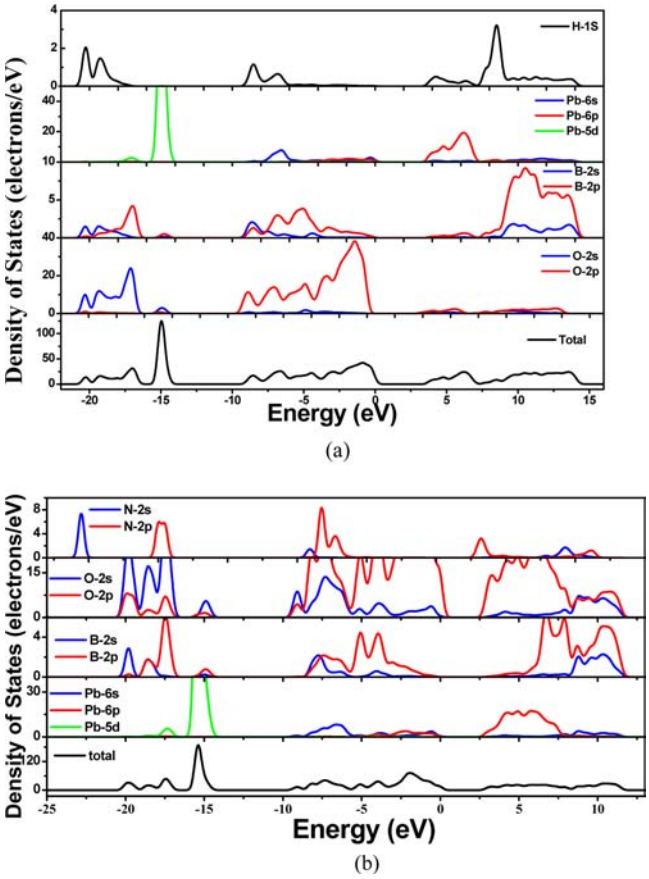

Figure 5. Electronic DOS of $Pb_2B_3O_{5.5}(OH)_2$ (a) and $[Pb_3(B_3O_7)](NO_3)$ (b).

isolated Pb-5d. In the vicinity of the Fermi level, namely, from −8.6 to 0 eV in the valence band and from 4.1 to 6.3 eV in the conduction band, the O-2p, B-2s2p, Pb-6s6p, and H-1s states are all involved and overlap fully, indicative of the strong covalent interactions of Pb−O, B−O, and H−O bonds. The DOS curves of $[Pb_3(B_3O_7)](NO_3)$ are very similar to those of $Pb_2B_3O_{5.5}(OH)_2$ except the N−O bonding interactions. In addition, to further verify the stereoactive lone-pair electrons on the Pb^{2+} cation, the electron density difference map around the Pb^{2+} cation was calculated (Figure 6). The map describes well the polarization and charge transfer of the system and clearly reveals the asymmetric lobe on Pb^{2+}; hence the Pb^{2+}-$6s^2$ lone-pair electrons should be stereoactive.

CONCLUSIONS

In summary, a new polar material, namely, $Pb_2B_3O_{5.5}(OH)_2$, and the first example of the mixed-anion lead(II) borate nitrates, namely, $[Pb_3B_3O_7](NO_3)$, have been synthesized by simple hydrothermal reactions. Though $Pb_2B_3O_{5.5}(OH)_2$ contains only BO_4 tetrahedra, because of the synergistic polarization effects of the lone pairs of the lead(II) cations, it still exhibits a strong second-harmonic generation response of about 3.0 × KDP which is type I phase-matchable. Results of our work demonstrate that a series of lead(II) borates can be prepared in a high yield by using a clean and facile method. With lead(II) metaborate as the starting materials, by only adjusting pH value of reaction system, four different borates were obtained, which indicates that the borate system is very sensitive to the experimental conditions. Further research

dx.doi.org/10.1021/ic401175r | Inorg. Chem. 2013, 52, 8979−8986

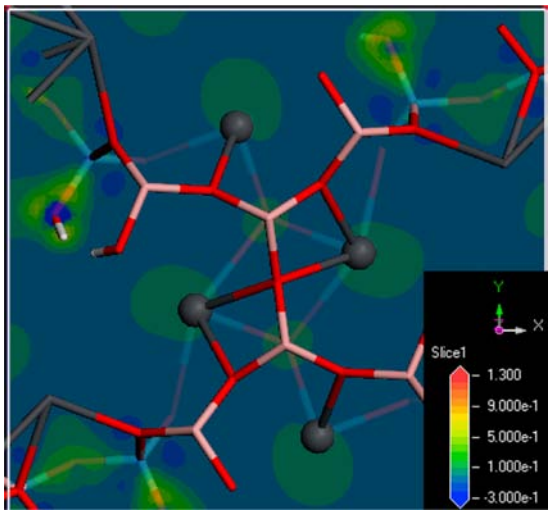

Figure 6. Electron density difference map around the lead(II) ion in $Pb_2B_3O_{5.5}(OH)_2$ (The gray balls represent Pb atoms).

efforts will be devoted to the preparations and characterizations of other metal borates by using similar synthetic techniques.

■ ASSOCIATED CONTENT

Supporting Information

X-ray crystallographic files in CIF format, simulated and experimental XRD patterns, IR, UV absorption, optical diffuse reflectance spectra, and TGA data for both compounds, and figures showing the plarization directions of the lead(II) ion in $Pb_2B_3O_{5.5}(OH)_2$. This material is available free of charge via the Internet at http://pubs.acs.org.

■ AUTHOR INFORMATION

Corresponding Author

*E-mail: mjg@fjirsm.ac.cn. Fax: (+86)591-83714946.

Notes

The authors declare no competing financial interest.

■ ACKNOWLEDGMENTS

This work was supported by the National Natural Science Foundation of China (Nos.2123006, 21001107 and 2120319).

■ REFERENCES

(1) (a) Ok, K. M.; Chi, E. O.; Halasyamani, P. S. *Chem. Soc. Rev.* **2006**, *35*, 710. (b) Chen, C.-T.; Liu, G.-Z. *Annu. Rev. Mater. Sci.* **1986**, *16*, 203.

(2) (a) Becker, P. *Adv. Mater.* **1998**, *10*, 979. (b) Chen, C. T.; Wang, Y. B.; Wu, B. C.; Wu, K. C.; Zeng, W. L.; Yu, L. H. *Nature* **1995**, *373*, 322. (c) Chen, C. T.; Wu, B. C.; Jiang, A. D.; You, G. M. *Sci. Sin., Ser. B* **1984**, *14*, 598. (d) Hagerman, M. E.; Poeppelmeier, K. R. *Chem. Mater.* **1995**, *7*, 602. (e) Wu, H. P.; Pan, S. L.; Poeppelmeier, K. R.; Li, H. Y.; Jia, D. Z.; Chen, Z. H.; Fan, X. Y.; Yang, Y.; Rondinelli, J. M.; Luo, H. S. *J. Am. Chem. Soc.* **2011**, *133*, 7786.

(3) (a) Dmitriev, V. G.; Gurzadyan, G. G.; Nikogosyan, D. N. *Handbook of Nonlinear Optical Crystals*; Springer: Berlin, Germany, 1991. (b) Boyd, G. D.; Buehler, E.; Storz, F. G. *Appl. Phys. Lett.* **1971**, *18*, 301. (c) Liao, J. H.; Marking, G. M.; Hsu, K. F.; Matsushita, Y.; Ewbank, M. D.; Borwick, R.; Cunningham, P.; Rosker, M. J.; Kanatzidis, M. G. *J. Am. Chem. Soc.* **2003**, *125*, 9484. (d) Zhang, Q.; Chung, I.; Jang, J. I.; Ketterson, J. B.; Kanatzidis, M. G. *J. Am. Chem. Soc.* **2009**, *131*, 9896.

(4) (a) Ye, N.; Chen, Q. X.; Wu, B. C.; Chen, C. T. *J. Appl. Phys.* **1998**, *84*, 555. (b) Chen, C. T.; Wu, Y. C.; Li, R. K. *Int. Rev. Phys. Chem.* **1989**, *8*, 65. (c) Zou, G. H.; Ye, N.; Huang, L.; Lin, X. S. *J. Am. Chem. Soc.* **2011**, *133*, 20001. (d) Tran, T. T.; Halasyamani, P. S. *Inorg Chem.* **2013**, *52*, 2466. (e) Cong, R. H.; Yang, T.; Liao, F. H.; Wang, Y. X.; Lin, Z. S.; Lin, J. H. *Mater. Res. Bull.* **2012**, *47*, 2573. (f) Kim, M. K.; Jo, V.; Ok, K. M. *Inorg. Chem.* **2009**, *48*, 7368.

(5) (a) Yu, H. W.; Pan, S. L.; Wu, H. P.; Zhao, W. W.; Zhang, F. F.; Li, H. Y.; Yang, Z. H. *J. Mater. Chem.* **2012**, *22*, 2105. (b) Rastsvetaeva, R. K.; Arakcheeva, A. V.; Pushcharovsky, D. Y.; Vinogradova, S. A.; Dimitrova, O. V.; Stefanovich, S. Y. *Z. Kristallogr.* **1998**, *213*, 240.

(6) Huppertz, H. *Chem. Commun.* **2011**, *47*, 131.

(7) Kong, F.; Huang, S. P.; Sun, Z. M.; Mao, J. G.; Cheng, W. D. *J. Am. Chem. Soc.* **2006**, *128*, 7750.

(8) Huang, Y. Z.; Wu, L. M.; Wu, X. T.; Li, L. H.; Chen, L.; Zhang, Y. F. *J. Am. Chem. Soc.* **2010**, *132*, 12788.

(9) Zhang, W. L.; Cheng, W. D.; Zhang, H.; Geng, L.; Lin, C. S.; He, Z. Z. *J. Am. Chem. Soc.* **2010**, *132*, 1508.

(10) Zou, G. H.; Zhang, L. Y.; Ye, N. *CrystEngComm* **2013**, *15*, 2422.

(11) Burns, P. C.; Grice, J. D.; Hawthorne, F. C. *Can. Mineral.* **1995**, *33*, 1131.

(12) Yu, Z. T.; Shi, Z.; Jiang, Y. S.; Yuan, H. M.; Chen, J. S. *Chem. Mater.* **2002**, *14*, 1314.

(13) Corker, D. L.; Glazer, A. M. *Acta Crystallogr., Sect. B* **1996**, *52*, 260.

(14) (a) Oseledchik, Y. S.; Prosvirnin, A. L.; Pisarevskiy, A. I.; Starshenko, V. V.; Osadchuk, V. V.; Belokrys, S. P.; Svitanko, N. V.; Korol, A. S.; Krikunov, S. A.; Selevich, A. F. *Opt. Mater.* **1995**, *4*, 669. (b) Nicholls, J. F. H.; Chai, B. H. T.; Russell, D.; Henderson, B. *Opt. Mater.* **1997**, *8*, 185.

(15) Jeggo, C. R. D.Phil. Thesis, St Catherine's College, Oxford, England, 1971.

(16) (a) Li, L. Y.; Jin, X. L.; Li, G. B.; Wang, Y. X.; Liao, F. H.; Yao, G. Q.; Lin, J. H. *Chem. Mater.* **2003**, *15*, 2253. (b) Li, L. Y.; Li, G. B.; Wang, Y. X.; Liao, F. H.; Lin, J. H. *Chem. Mater.* **2005**, *17*, 4174. (c) Wang, S. A.; Alekseev, E. V.; Depmeier, W.; Albrecht-Schmitt, T. E. *Chem. Commun.* **2010**, *46*, 3955. (d) Polinski, M. J.; Alekseev, E. V.; Darling, V. R.; Cross, J. N.; Depmeier, W.; Albrecht-Schmitt, T. E. *Inorg. Chem.* **2013**, *52*, 1965. (e) Polinski, M. J.; Grant, D. J.; Wang, S.; Alekseev, E. V.; Cross, J. N.; Villa, E. M.; Depmeier, W.; Gagliardi, L.; Albrecht-Schmitt, T. E. *J. Am. Chem. Soc.* **2012**, *134*, 10682. (f) Polinski, M. J.; Wang, S.; Cross, J. N.; Alekseev, E. V.; Depmeier, W.; Albrecht-Schmitt, T. E. *Inorg. Chem.* **2012**, *51*, 7859.

(17) Williams, I. D.; Wu, M. M.; Sung, H. H-Y.; Zhang, X. X.; Yu, J. H. *Chem. Commun.* **1998**, 2463.

(18) Sun, C. F.; Hu, C. L.; Xu, X.; Kong, F.; Mao, J. G. *J. Am. Chem. Soc.* **2011**, *133*, 5561.

(19) Zhou, Y.; Fang, C.; Fang, Y.; Zhu, F. *Spectrochim. Acta, Part A* **2011**, *83*, 82.

(20) Wendlandt, W. M.; Hecht, H. G. *Reflectance Spectroscopy*; Interscience: New York, 1966.

(21) Kutz, S. K.; Perry, T. T. *J. Appl. Phys.* **1968**, *39*, 3798.

(22) (a) *CrystalClear*, Version 1.3.5; Rigaku Corp.: Woodlands, TX, 1999. (b) Sheldrick, G. M. *SHELXTL, Crystallographic Software Package, SHELXTL*, Version 5.1; Bruker-AXS: Madison, WI, 1998. (c) Spek, A. L. *J. Appl. Crystallogr.* **2003**, *36*, 7.

(23) (a) Brown, I. D.; Altermatt, D. *Acta Crystallogr., Sect. B* **1985**, *41*, 244. (b) Brese, N. E.; O'Keeffe, M. *Acta Crystallogr., Sect. B* **1991**, *47*, 192.

(24) (a) Segall, M. D.; Lindan, P. J. D.; Probert, M. J.; Pickard, C. J.; Hasnip, P. J.; Clark, S. J.; Payne, M. C. *J. Phys.: Condens. Matter* **2002**, *14*, 2717. (b) Milman, V.; Winkler, B.; White, J. A.; Pickard, C. J.; Payne, M. C.; Akhmatskaya, E. V.; Nobes, R. H. *Int. J. Quantum Chem.* **2000**, *77*, 895.

(25) Perdew, J. P.; Burke, K.; Ernzerhof, M. *Phys. Rev. Lett.* **1996**, *77*, 3865.

(26) Lin, J. S.; Qteish, A.; Payne, M. C.; Heine, V. *Phys. Rev. B* **1993**, *47*, 4174.

(27) Blatov, V. A. *IUCr CompComm Newslett.* **2006**, *7*, 4; http://www.topos.ssu.samara.ru.

(28) Knyrim, J. S.; Schappacher, F. M.; PÖttgen, R.; Günne, J. S.; Johrendt, D.; Huppertz, H. *Chem. Mater.* **2007**, *19*, 254.
(29) (a) Maggard, P. A.; Nault, T. S.; Stern, C. L.; Poeppelmeier, K. R. *J. Solid State Chem.* **2003**, *175*, 27. (b) Izumi, H. K.; Kirsch, J. E.; Stren, C. L.; Poeppelmeier, K. R. *Inorg. Chem.* **2005**, *44*, 884. (c) Sivakumar, T.; Chang, H. Y.; Baek, J.; Halasyamani, P. S. *Chem. Mater.* **2007**, *19*, 4710.
(30) Sun, C. F.; Hu, C. L.; Mao, J. G. *Chem. Commun.* **2012**, *48*, 4220.
(31) (a) Godby, R. W.; Schluter, M.; Sham, L. *J. Phys. Rev. B: Condens. Matter Mater. Phys.* **1987**, *36*, 6497. (b) Okoye, C. M. I. *J. Phys.: Condens. Matter* **2003**, *15*, 5945. (c) Terki, R.; Bertrand, G.; Aourag, H. *Microelectron. Eng.* **2005**, *81*, 514.